2021 43rd Annual International Conference of the
IEEE Engineering in Medicine & Biology Society (EMBC)
Oct 31 - Nov 4, 2021. Virtual Conference

UStEMG: an Ultrasound Transparent Tattoo-based sEMG System for Unobtrusive Parallel Acquisitions of Muscle Electro-mechanics

Christoph Leitner[1], Simone Benatti[2], Kirill Keller[3], Andrea Cossettini[4], Victor Kartsch[2], Harald Penasso[5], Luca Benini[2,4], Francesco Greco[3], Christian Baumgartner[1]

***Abstract*— Human machine interfaces follow machine learning approaches to interpret muscles states, mainly from electrical signals. These signals are easy to collect with tiny devices, on tight power budgets, interfaced closely to the human skin. However, natural movement behavior is not only determined by muscle activation, but it depends on an orchestration of several subsystems, including the instantaneous length of muscle fibers, typically inspected by means of ultrasound (US) imaging systems. This work shows for the first time an ultra-lightweight (7 g) electromyography (sEMG) system transparent to ultrasound, which enables the simultaneous acquisition of sEMG and US signals from the same location. The system is based on ultrathin and skin-conformable temporary tattoo electrodes (TTE) made of printed conducting polymer, connected to a tiny, parallel-ultra-low power acquisition platform (BioWolf). US phantom images recorded with the TTE had mean axial and lateral resolutions of 0.90 ± 0.02 mm and 1.058 ± 0.005 mm, respectively. The root mean squares for sEMG signals recorded with the US during biceps contractions were at 57 ± 10 μV and mean frequencies were at 92 ± 1 Hz. We show that neither ultrasound images nor electromyographic signals are significantly altered during parallel and synchronized operation.**

***Clinical relevance*— Modern prosthetic engineering concepts use interfaces connected to muscles or nerves and employ machine learning models to infer on natural movement behavior of amputated limbs. However, relying only on a single data source (e.g., electromyography) reduces the quality of a fine-grained motor control. To address this limitation, we propose a new and unobtrusive device capable of capturing the electrical and mechanical behavior of muscles in a parallel and synchronized fashion. This device can support the development of new prosthetic control and design concepts, further supporting clinical movement science in the configuration of better simulation models.**

I. INTRODUCTION

System level observations of human movement reveal that voluntary contractions of muscles are electrochemically provoked by neural inputs which are initiated in the brain. In turn, these contractions generate forces that are mechanically transferred (via tendons) over joints causing joint torques and movement. Muscle force depends on the grade of muscle activation [1], on muscle and sarcomere length [2], on muscle contraction velocity [3], on contraction mode (isometric, concentric, eccentric) [4], and on contraction history [5]. In laboratory conditions and during human movement surface electromyography (sEMG) and ultrasound (US) are used to quantify the state of a muscle during a contraction.

At present, sEMG is a widely used method to detect and evaluate muscle activation [6]. Thanks to its unobtrusive design and low cost compared to other medical modalities, it is increasingly used for human machine interface (HMI) controls [7] and found its way into the consumer market (e.g. prosthetic control [8]). As equal levels of muscle activation can be reached at different mechanical and physiological states [9], controlling HMIs only by means of activation signals, might impede a precise and fluent mimicking of human motor controls [10], [11]. Hence, research has started to incorporate activation and instantaneous length of muscles as input parameters for structural muscle models [12], or the control of powered prosthetics [13]. Among the possible approaches to record and evaluate tissue mechanics during human movement, ultrasound (US) has emerged as a powerful tool [14]–[17]. Botter et al. [18] have demonstrated parallel acquisitions of US and sEMG during stimulated muscle twitch. Their system consists of a silicon rag (> 4 mm thickness), fastened with elastic bands to the region of interest. Conductive gel is used to guarantee sEMG signal transmission from the skin to the integrated stainless steel wire electrodes. They were able to show fascicle length changes and M-waves of the same muscle area during stimulation. However, their device does not meet the requirements of a wearable system in general [19]–[21].

Recently, ultra-thin temporary tattoo electrodes (TTEs) have been proposed as transducers for surface electrophysiology applications such as EMG, ECG, EEG recordings [22], [23], respiration monitoring [24], or the myographic control of prosthetics [25]. In contrast to conventional skin-electrodes, TTEs are skin-conformable and unperceivable, as they are closely adhering to the skin and require no gel interface nor any other skin preparations [23]. The all-polymer nature of TTE suggests US transparency and makes it a good candidate for simultaneous, unhindered sEMG and US signal acquisition during movement.

Within this context, our work *demonstrates an ultra-lightweight (7 g) sEMG system with miniaturized acquisition hardware and comfortable US-transparent epidermal tattoo electrodes for concurrent and precisely synchronized US and sEMG analysis of muscle motion.* Our US phantom images

[1]Institute of Health Care Engineering with European Testing Center for Medical Devices, Graz University of Technology, 8010 Graz, Austria. Correspondence: christoph.leitner@tugraz.at

[2]Department of Electrical and Electronic Engineering, University of Bologna, 40136 Bologna, Italy.

[3]Institute of Solid State Physics, Graz University of Technology, 8010 Graz, Austria.

[4]Integrated Systems Laboratory, ETH Zürich, 8092 Zürich, Switzerland.

[5]Department of Integrative Physiology, University of Colorado Boulder, Boulder, CO, USA

This work is licensed under a Creative Commons Attribution 3.0 License.
For more information, see http://creativecommons.org/licenses/by/3.0/

recorded with the TTE had mean axial and lateral resolutions of 0.90 ± 0.02 and 1.058 ± 0.005 mm, respectively. Root mean squares for sEMG signals recorded with the US during biceps contractions were at 57 ± 10 μV and mean frequencies were at 92 ± 1 Hz. We demonstrate that neither ultrasound images nor sEMG signals are significantly altered during a parallel acquisition of the muscle electro-mechanics using our device.

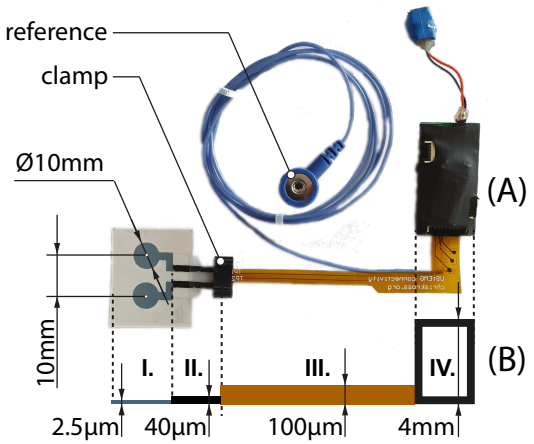

Fig. 1. (A) UStEMG System Components: **I.** printed TTEs, **II.** conductive laser induced graphene (LIG) tracks, **III.** flexible printed circuit board (PCB) interface, **IV.** BioWolf 8-channel acquisition platform. (B) Schematic representation (not in scale) of the thickness and material properties of the individual components.

II. MATERIALS AND METHODS

A. System components

Fig. 1 shows the main components of the ultrasound transparent sEMG (UStEMG) system. TTEs (Fig. 1, I.) were used as transducers interfacing the skin to collect sEMG signals. TTEs were fabricated by screen printing of conducting polymer poly(3,4-ethylenedioxythiophene) polystyrene sulfonate (PEDOT:PSS) on top of commercially available temporary tattoo paper, as described in [26]. Printed TTEs were designed in compliance with the SENIAM guidelines [27], [28]. They had a round shape with a diameter of 10 mm and an interelectrode distance of 10 mm. External connection from the skin-adhered TTEs to the flexible PCB (Fig. 1, III.) was provided through soft and stretchable interconnectors based on conductive laser induced graphene (LIG). These LIG liners were embedded into a two-layered polyurethane medical adhesive (Fig. 1 II.), prepared as described in [29]. High electro-mechanical performance of these interconnectors provided sufficient mechanical stability during movement. We used a 100 µm thick flexible PCB board (Fig. 1, III.) which connected the TTEs and the 8–channel acquisition platform (BioWolf) [30] (Fig. 1, IV.). The complete 1 channel system had a span of 140 mm x 80 mm and a weight of 7 g. The thickness of the components gradually increased from ∼2.5 µm (for the TTEs) to approx. 4 mm (for the acquisition platform), as depicted in Fig. 1 (B). If needed, a reference electrode and an additional channel could be directly soldered on the flexible connector.

B. Analysis of ultrasound signals

As a first step to assess the quality of our ultrasound transparent sEMG system (UStEMG), we evaluated if the TTEs impaired the ultrasonic signals. This assessment was done by comparing contrast-to-noise ratio (CNR) and axial/lateral resolution of US images, with and without the TTE. Fig. 2 (A) shows the measurement setup. We used a portable US system Mindray M5 (Mindray, Guangdong, China) for US excitation and readout. The system was connected to a linear array transducer (Mindray 7L4s) operated at 7.5 MHz. A general purpose US phantom model 054GS (CIRS, Norfolk, Virginia, USA) was used for assessing the system performance in terms of resolution and contrast-to-noise ratio. The transducer probe was positioned on a selected area of the phantom, in order to image resolution targets and hyper-echogenic areas, and we recorded $n = 20$ images. A TTE was then attached on the phantom surface (Fig. 2, B) by gently pressing the TTE against the phantom and wetting the support paper. This caused the dissolution of the sacrificial starch layer and a conformal adhesion of the TTE. Then we recorded another set of $n = 20$ images.

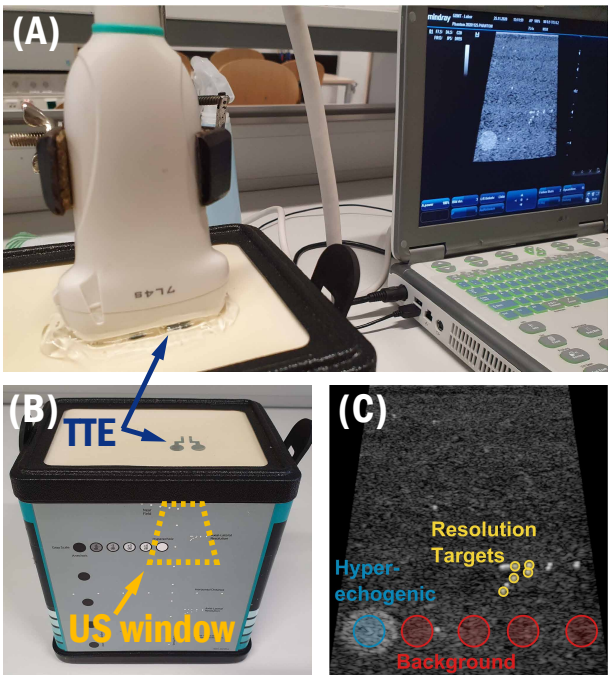

Fig. 2. (A) General setup of the US image acquisition on the CIRS general purpose phantom. The placement of the TTE underneath the ultrasonic lens is indicated with the blue arrows. (B) CIRS phantom with the TTE placed on its surface (blue arrows). The recorded ultrasonic window is indicated as an orange box. (C) Reconstructed image of one acquisition. The areas used for the calculation of the contrast-to-noise ratio (hyperechogenic and background) and the point targets for assessing axial and lateral resolutions are marked in blue, red, and yellow, respectively.

For both setups (with and without the TTE), the maximum imaging depth was 4.5 cm and included 4 focal positions at 1.25, 2, 2.75 and 3.75 cm. Specific circular target areas in US images were selected using binary masks. To calculate the CNR, we considered one region in the hyperechogenic area (blue circle in Fig. 2, C) and $m = 4$ regions of the

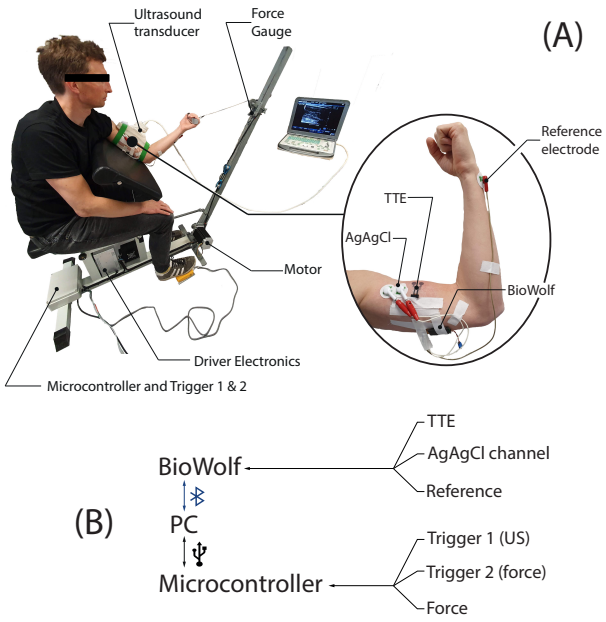

Fig. 3. (A) Experimental setup on the biceps test bench and all involved sensors and systems. TTE, conventional sEMG electrodes, and an ultrasound probe are placed on the biceps brachii of a healthy volunteer. (B) Schematic representation of the test bench and triggers.

same size and at the same depth on the image background (red circles in Fig. 2, C, representing different choices of the background area). The mean CNR (over n image samples) was then computed as:

$$CNR = \sum_{i=1}^{n} \frac{1}{n} \sum_{j=1}^{m} \frac{1}{m} 20 \log_{10} \left(\frac{|\mu_{(echo)_i} - \mu_{(bgr)_{ij}}|}{\sqrt{(\sigma^2_{(echo)_i} + \sigma^2_{(bgr)_{ij}})/2}} \right) [dB] \quad (1)$$

where $\mu_{(echo)_i}$ and $\sigma_{(echo)_i}$ were the mean and standard deviation grey levels within the hyper-echogenic region (blue circle in Fig. 2, C) for the i-th image, and $\mu_{(bgr)_{ij}}$ and $\sigma_{(bgr)_{ij}}$ were the mean and standard deviation grey levels within the j-th background region (the four red circles in Fig. 2, C) again for the i-th image. To calculate the image resolutions in axial and lateral directions, we selected several point targets in the US image (yellow points in Fig. 2, C) and calculated the full width at half maximum (FWHM) along the axial and lateral direction.

C. Analysis of electromyographic signals

As a second step to assess the quality of UStEMG, we evaluated if the ultrasonic waves influenced the acquisition of sEMG data.

Experimental data collection

We used the testbench shown in Fig. 3 to measure sEMG signals on the biceps brachii (BB) of a healthy volunteer. The test subject is held on a handlebar equipped with a force gauge and connected to a stepper motor that applied torque during isometric BB contractions. The TTE was positioned on the BB according to the Seniam guidelines [27]. A second Ag/AgCl electrode channel was applied on the far proximal-medial end of the BB, for signal-debugging during experimental recordings. The BioWolf system was attached to the skin of the participant with adhesive tape (Fig. 3 A, right inset). After placing the sEMG-electrodes, we used a custom-made styrofoam cast and securely attached the US transducer centered on top of the TTE.

Fig. 4 shows a sketch of the two measurement protocols followed for these evaluations. We captured the sEMG signals during muscle contraction and in resting state (i.e., to measure sEMG baseline and noise level), with or without activating the US probe, therefore covering a total of four measurement phases. We controlled signal recording times via a running clock and captured approx. 10s for each individual signal portion.

Hardware synchronization

To synchronize all recording devices, we used 2 analog triggers (Joy-it SEN-Pressure02, SIMAC Electronics, Germany) with pressure sensitive tips (maximum response time $<$1 ms). Both triggers acted as masters for the BioWolf service running on the PC subsystem. One trigger was placed on the US start button and additionally switched the US on or off. The second trigger was placed beside the US (for ease of access by the user) and further managed the force-control, without interfering with the US. Both triggers were connected to a microcontroller (8-bit AVR ATmega32U4, Microchip Technology Inc., Chandler, Arizona, USA) located on the instrumented testbench. The internal analog-to-digital converter (ADC) clock of the microcontroller was set to 125 kHz and each conversion took 13 ADC clocks. The SPI Bus connected the microcontroller with the PC and operated at a baudrate of 9.6 kBd. Hence, detecting the rising edge coming from the pressure sensor and transferring one 8-bit sample to the BioWolf service running on the PC resulted in a trigger latency $<$2 ms.

Signal processing

Signal processing was implemented in MATLAB (The Mathworks, Natick, MA, USA). Raw sEMG channel traces

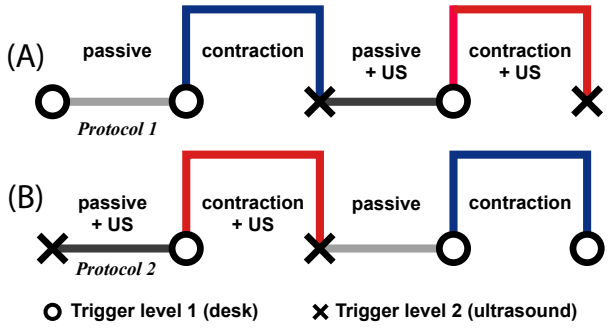

Fig. 4. Implemented protocols of sEMG measurements. The series of acquisitions were: (a) relaxed BB (i.e., measurement of sEMG noise), controlled muscle contraction (i.e., measurement of sEMG signal), relaxed BB with US probe activated (i.e., measurement of sEMG noise with US activation), controlled muscle contraction with US probe activated (i.e., measurement of sEMG signal with US activation). (b) same as (a), inverting the order of the first and last two phases. Two distinct triggers (trigger 1 and trigger 2) were used to activate/deactivate the force/sEMG and the US systems, respectively.

were filtered with a 4^{th} order Butterworth band-pass filter with cut-off frequencies at f_{low} = 20 Hz and f_{high} = 320 Hz. We evaluated amplitude and spectral features of the sEMG signals based on the methodology proposed by Farina et al. [31]. Firstly, we compensated the subject muscle response time by applying a -250 ms delay [32], [33] on the signals. Then, the channel traces were split according to the protocol stages shown in Fig. 4. To this end, the recorded trigger levels were used as a Boolean mask on top of the sEMG signals to identify the signal portions that belong to each individual phase. Finally, to compare sEMG amplitudes, we calculated the root mean square (RMS) of each sEMG signal portion. Moreover, mean signal-to-noise ratios (over n samples) were computed as:

$$SNR = \sum_{i=1}^{n} \frac{1}{n} 20 \log_{10} \left(\frac{RMS_{(contraction)_{ij}}}{RMS_{(passive)_{ij}}} \right) [dB] \qquad (2)$$

where $RMS_{(contraction)_{ij}}$ and $RMS_{(passive)_{ij}}$ were the RMS values for the i-th phase pair (contraction/passive) for the j-th protocol.

Welch's method [34] was used to estimate spectral densities of the recorded signal stages. We calculated the mean frequency (MNF) of each received signal spectra for further statistical analysis. In the following, we considered signals collected during both protocols, with and without active US, using RMSs and MNFs as metrics for comparison.

Statistical data analysis

Statistical data analyses were implemented in Python (Python Foundation, Delaware, USA) using *scipy* and the statistical parameter mapping package *spm1d* [35] for 1D time dependent data. We used a two sample t-test to test against the null hypothesis. The minimum level of statistical significance was set at $p < 0.05$. Values are presented as mean and standard deviation.

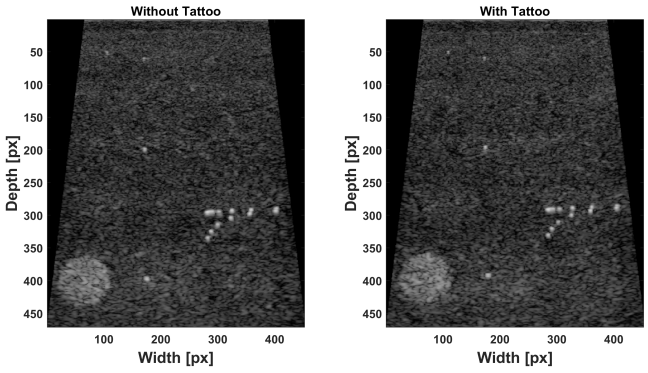

Fig. 5. Comparison of ultrasound images without and with the TTE.

TABLE I
QUANTITATIVE COMPARISON OF ULTRASOUND IMAGES

Configuration	CNR [dB]	Resolution	
		Axial [mm]	Lateral [mm]
without TTE	5.31 ± 0.04	0.94 ± 0.04	0.942 ± 0.007
with TTE	4.35 ± 0.05	0.90 ± 0.02	1.058 ± 0.005

III. RESULTS AND DISCUSSION

Fig. 5 shows the qualitative comparison between the US images without (left) and with the TTE (right), as measured on the phantom. The two images are generated with the same dynamic-range scale. While the resolution point targets appear almost unaltered, slight differences in the contrast can be appreciated. Table I reports a quantitative assessment of the CNR and the axial and lateral resolutions for both configurations (without and with the TTE), for measurements on the phantom. The numbers in the table are reported as mean and standard deviation values, calculated over 20 distinct images. The presence of TTE induced negligible degradations in the axial and lateral resolution. The CNR is reduced by approx. 20%, a drop that does not hamper the proper identification of the target objects.

Table II reports a quantitative assessment of differences between the sEMG acquisitions with and without ultrasound during both protocols. The null-hypothesis was never rejected for any of the RMS and MNF pairs: passive without - passive with US, contraction without - contraction with US in both protocols. Fig. 6 (top) shows one representative sEMG trace, as captured with the setup of Fig. 3 following protocol 1 (see Fig. 4). Fig. 6 (center) shows a zoom-in over the transition from noise to signal (i.e., muscle relaxation to muscle contraction) phase, collected with and without the ultrasound signal activated. We compared 12 sEMG signal traces collected with ultrasound and other 12 traces collected without US and find no significant effect for ultrasound on sEMG signals ($t(22)=4.27$, $p>0.05$) using statistical parameter mapping. Fig. 6 (bottom) shows the corresponding power spectrum. Although the power distribution around the MNF is higher for traces collected with US, there was no significant difference in MNFs ($t(22)=0.23$, $p=0.82$) between the collections with and without the ultrasound. Furthermore, we compared SNRs (Table II) which show no significant effect for ultrasound in protocol 1 ($t(10)=0.09$, $p=0.92$) and protocol 2 ($t(10)=0.01$, $p=0.98$).

Ultimately we could demonstrate that neither the ultrasound images nor the sEMG signals are significantly altered by the presence of the TTE and US, respectively. However, it is still unclear how sEMG signals are affected by a reduction in size of the TTEs, or by changes in inter-electrode distances. A reduction of both measures could pave

TABLE II
AMPLITUDE AND SPECTRAL ANALYSIS OF EMG SIGNALS

	Phase	RMS [µV]	MNF [Hz]	SNR [dB]
protocol 1	**Passive w/o US**	6 ± 3	85 ± 6	20 ± 4
	Contraction w/o US	58 ± 7	93 ± 1	
	Passive w/ US	7 ± 4	88 ± 4	19 ± 2
	Contraction w/ US	64 ± 13	92 ± 2	
protocol 2	**Passive w/ US**	6 ± 2	81 ± 11	19 ± 3
	Contraction w/ US	50 ± 8	91 ± 1	
	Passive w/o US	6 ± 2	87 ± 3	19 ± 3
	Contraction w/o US	56 ± 6	91 ± 2	

White background: without US. | Grey background: with US.

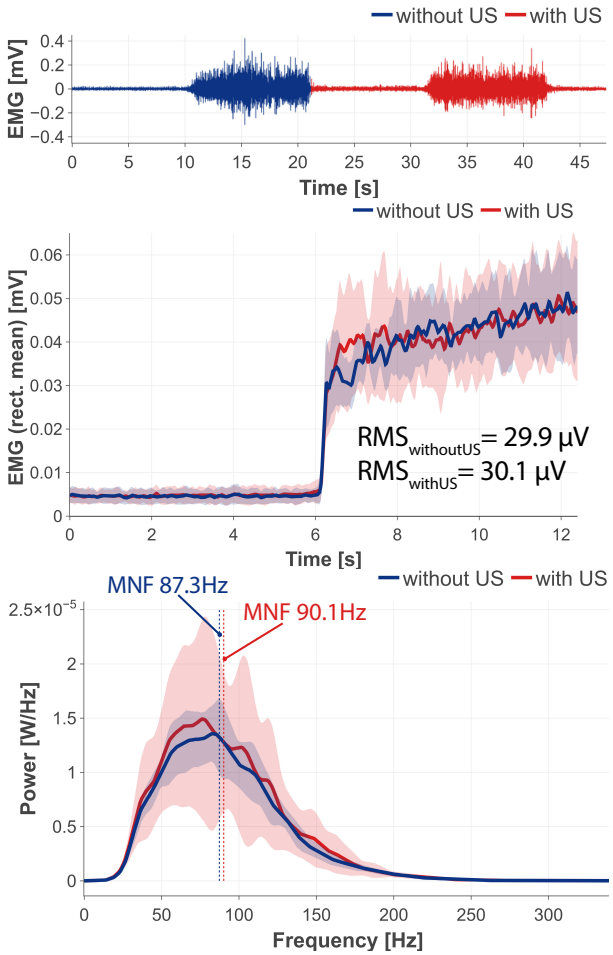

Fig. 6. Top: a representative sEMG signal trace from protocol 1. The blue color indicates the sEMG recording without ultrasound. Traces collected with the ultrasound are in red color. Center: comparison between rectified mean amplitudes of the sEMG recrodings with (red) and without (blue) ultrasound. Bottom: comparison of frequency spectra of sEMG recordings with and without ultrasound. Mean frequencies of each spectrum are indicated as dotted lines.

the way to larger high density electrode grids, allowing the collection of sEMG signals and action potential dynamics under the full US aperture and within a high density grid. Furthermore, and in context of HMIs, a continuous collection of both US and sEMG signals would be favorable. Hence, further research should also target possible signal degradation in medium to long-term applications.

IV. CONCLUSIONS

HMIs are typically data-driven and employ mostly electrical signals collected from peripherals or brain for operation. However, motor controls in vertebrate are complex and naturally several subsystems need to be orchestrated to form movement behaviour. Therefore, synchronized recordings of both the electrical activation and mechanical response of muscles could support machine learning approaches to interpret muscle states. Our work demonstrates an ultra-lightweight (7 g) sEMG system capable of parallel acquisitions of ultrasound and sEMG to detect muscle mechanics and their activation, respectively. We show that the sEMG signals are not impeded by the presence of ultrasound signals. Furthermore, we demonstrate that ultrasound images are not significantly altered by the presence of skin adhesive PEDOT:PSS tattoo electrodes.

ACKNOWLEDGMENT

The authors thank S. Vostrikov for fruitful discussions. C. Leitner would like to acknowledge Martin Sust (University of Graz) for the support of his research.

REFERENCES

[1] N. Bernstein, "The Co-ordination and Regulation of Movements." *Science*, vol. 159, no. 3813, pp. 415–416, 1 1968.

[2] A. M. Gordon, A. F. Huxley, and F. J. Julian, "The variation in isometric tension with sarcomere length in vertebrate muscle fibres," *J. Physiol.*, vol. 184, no. 1, pp. 170–192, 5 1966.

[3] A.V. Hill, "The heat of shortening and the dynamic constants of muscle," *Proc. of the Royal Society of London*, vol. 126, no. 843, pp. 136–195, 10 1938.

[4] A. J. Van Soest and M. F. Bobbert, "The contribution of muscle properties in the control of explosive movements." *Biological Cybernetics*, vol. 69, no. 3, pp. 195–204, 1993.

[5] W. Herzog, "History dependence of skeletal muscle force production: implications for movement control." *Human Movement Science*, vol. 23, no. 5, pp. 591–604, 2004.

[6] C. J. De Luca, "The use of surface electromyography in biomechanics," in *J. Appl. Biomech.*, vol. 13, no. 2. Human Kinetics Publishers Inc., 5 1997, pp. 135–163.

[7] S. Benatti, F. Casamassima, B. Milosevic, E. Farella, P. Schönle, S. Fateh, T. Burger, Q. Huang, and L. Benini, "A Versatile Embedded Platform for EMG Acquisition and Gesture Recognition," *IEEE Trans. Biomed. Circuits Syst.*, vol. 9, no. 5, pp. 620–630, 10 2015.

[8] "Myoelectric prosthetics 101 — Ottobock US." [Online]. Available: https://www.ottobockus.com/prosthetics/info-for-new-amputees/prosthetics-101/myoelectric-prosthetics-101/

[9] R. Merletti and D. Farina, *Surface Electromyography: Physiology, Engineering and Applications*, 1st ed., R. Merletti and D. Farina, Eds. Piscataway: Wiley-IEEE Press, 2016.

[10] K. Nishikawa, A. A. Biewener, P. Aerts, A. N. Ahn, H. J. Chiel, M. A. Daley, T. L. Daniel, R. J. Full, M. E. Hale, T. L. Hedrick, A. K. Lappin, T. R. Nichols, R. D. Quinn, R. A. Satterlie, and B. Szymik, "Neuromechanics: An integrative approach for understanding motor control," *Integr. Comp. Biol.*, vol. 47, no. 1, pp. 16–54, 7 2007.

[11] T. J. Roberts and A. M. Gabaldón, "Interpreting muscle function from EMG: Lessons learned from direct measurements of muscle force," *Integr. Comp. Biol.*, vol. 48, no. 2, pp. 312–320, 8 2008.

[12] K. C. Nishikawa, J. A. Monroy, T. E. Uyeno, S. H. Yeo, D. K. Pai, and S. L. Lindstedt, "Is titin a 'winding filament'? A new twist on muscle contraction," *Proceedings of the Royal Society B: Biological Sciences*, vol. 279, no. 1730, pp. 981–990, 2012.

[13] A. Forner-Cordero, J. R. Jeffers, K. C. Nishikawa, U. Tahir, A. L. Hessel, E. R. Lockwood, J. T. Tester, Z. Han, D. J. Rivera, K. L. Covey, T. G. Huck, and N. A. Rice, "Case Study: A Bio-Inspired Control Algorithm for a Robotic Foot-Ankle Prosthesis Provides Adaptive Control of Level Walking and Stair Ascent," *Front. Rob. AI*, vol. 1, p. 36, 2018.

[14] G. Lichtwark, "Ultrasound Technology for Examining the Mechanics of the Muscle, Tendon, and Ligament," in *Handbook of Human Motion*. Springer International Publishing, 2017, pp. 1–20.

[15] M. Tanter, J. Bercoff, L. Sandrin, and M. Fink, "Ultrafast compound imaging for 2-D motion vector estimation: application to transient elastography," *IEEE Trans. Ultrason., Ferroelectr., Freq. Control*, vol. 49, no. 10, pp. 1363–1374, 10 2002.

[16] C. Leitner, S. Vostrikov, H. Penasso, P. A. Hager, A. Cossettini, L. Benini, and C. Baumgartner, "Detection of Motor Endplates in Deep and Pennate Skeletal Muscles in-vivo using Ultrafast Ultrasound," in *Proc. IEEE-IUS)*, 2020.

[17] C. Leitner, S. Vostrikov, M. Tilp, P. A. Hager, A. Cossettini, L. Benini, and C. Baumgartner, "Human Fascicle Strain Behavior During Twitch using Ultrafast Ultrasound," in *Proc. IEEE-IUS*, 2020.

[18] A. Botter, T. M. M. Vieira, I. D. Loram, R. Merletti, and E. F. Hodson-Tole, "A novel system of electrodes transparent to ultrasound for simultaneous detection of myoelectric activity and B-mode ultrasound images of skeletal muscles," *J. Appl. Physiol.*, vol. 115, no. 8, pp. 1203–1214, 10 2013.

[19] L. Benini, E. Farella, and C. Guiducci, "Wireless sensor networks: Enabling technology for ambient intelligence," *Microelectronics J.*, vol. 37, no. 12, pp. 1639–1649, 12 2006.

[20] Y. Liu, M. Pharr, and G. A. Salvatore, "Lab-on-Skin: A Review of Flexible and Stretchable Electronics for Wearable Health Monitoring," pp. 9614–9635, 10 2017.

[21] C. Leitner, P. A. Hager, H. Penasso, M. Tilp, L. Benini, C. Peham, and C. Baumgartner, "Ultrasound as a Tool to Study Muscle–Tendon Functions during Locomotion: A Systematic Review of Applications," *Sensors*, vol. 19, no. 19, p. 4316, 10 2019.

[22] L. M. Ferrari, S. Sudha, S. Tarantino, R. Esposti, F. Bolzoni, P. Cavallari, C. Cipriani, V. Mattoli, and F. Greco, "Ultraconformable Temporary Tattoo Electrodes for Electrophysiology," *Adv. Sci*, vol. 5, no. 3, p. 1700771, 3 2018.

[23] L. M. Ferrari, U. Ismailov, J. M. Badier, F. Greco, and E. Ismailova, "Conducting polymer tattoo electrodes in clinical electro- and magneto-encephalography," *npj Flexible Electron.*, vol. 4, no. 1, 12 2020.

[24] S. Taccola, A. Poliziani, D. Santonocito, A. Mondini, C. Denk, A. N. Ide, M. Oberparleiter, F. Greco, and V. Mattoli, "Toward the use of temporary tattoo electrodes for impedancemetric respiration monitoring and other electrophysiological recordings on skin," *Sensors*, vol. 21, no. 4, pp. 1–17, 2 2021.

[25] A. Zucca, C. Cipriani, Sudha, S. Tarantino, D. Ricci, V. Mattoli, and F. Greco, "Tattoo Conductive Polymer Nanosheets for Skin-Contact Applications," *Adv. Healthcare Mater.*, vol. 4, no. 7, pp. 983–990, 5 2015.

[26] L. M. Ferrari, K. Keller, B. Burtscher, and F. Greco, "Temporary tattoo as unconventional substrate for conformable and transferable electronics on skin and beyond," 9 2020.

[27] "Seniam guidlines." [Online]. Available: http://www.seniam.org/

[28] H. HJ, F. B, D.-K. C, and R. G, "Development of recommendations for SEMG sensors and sensor placement procedures," *Journal of electromyography and kinesiology : official journal of the International Society of Electrophysiological Kinesiology*, vol. 10, no. 5, pp. 361–374, 10 2000.

[29] A. Dallinger, K. Keller, H. Fitzek, and F. Greco, "Stretchable and Skin-Conformable Conductors Based on Polyurethane/Laser-Induced Graphene," *ACS Appl. Mater. Interfaces*, vol. 12, no. 17, pp. 19 855–19 865, 4 2020.

[30] V. Kartsch, G. Tagliavini, M. Guermandi, S. Benatti, D. Rossi, and L. Benini, "BioWolf: A Sub-10-mW 8-Channel Advanced Brain-Computer Interface Platform with a Nine-Core Processor and BLE Connectivity," *IEEE Trans. Biomed. Circuits Syst.*, vol. 13, no. 5, pp. 893–906, 10 2019.

[31] D. Farina and R. Merletti, "Comparison of algorithms for estimation of EMG variables during voluntary isometric contractions," *J. Electromyogr. Kinesiol.*, vol. 10, no. 5, pp. 337–349, 10 2000.

[32] J. P. Alvin Mojica, R. Nakamura, and Y. Yamada, "Effect of Reaction Time Condition on EMG Activities of the Biceps Brachii Muscle in Elbow Flexion and Forearm Supination," *Percept. Mot. Ski.*, vol. 67, pp. 807–813, 1988.

[33] K. Yotani, H. Nakamoto, S. Ikudome, and A. Yuki, "Muscle contraction and relaxation-response time in response to on or off status of visual stimulus," *J. Physiol. Anthropol.*, vol. 33, no. 1, 8 2014.

[34] P. Stoica and R. L. Moses, *Spectral analysis of signals*. Pearson/Prentice Hall, 2005.

[35] T. C. Pataky, "Generalized n-dimensional biomechanical field analysis using statistical parametric mapping," *J. Biomech.*, vol. 43, no. 10, pp. 1976–1982, 7 2010.